Chapter 4
TEC Plasticization of Topical Polymeric Films

The degree of homogeneity and the mechanical properties of topical polymeric films for drug delivery are vital to their efficacy. The dispersal of plasticizer and the solubility of the drug within the films (the homogeneity of their distribution) affect their function; phase separations have been shown to trigger drug crystallization [1] and the efficacy (bioavailability) and stability of the drug are dependent on its crystallinity [2]. Inhomogeneities may also provide weak points in the films where fracture is more likely [3]. If the mechanical properties of the film are similar to those of skin, it will flex with the skin and remain in intimate contact for a prolonged period of time. The incorporation of plasticizers into polymer films increases their flexibility [4] and permits the mechanical properties to be matched to those of skin. In this way, film breakage is avoided and the area across which drug transport occurs remains constant.

AFM and Raman chemical mapping have previously been used to determine the drug/polymer miscibility in polymeric films [1, 5]. The occurrence of drug crystallization was detected by the appearance of aggregates and worm-like structures in AFM images. AFM nanoindentation has been used to determine the form of drug particles, e.g., crystalline, and to what degree, or amorphous [6–8]. Raman mapping has been used as a complementary method to AFM allowing direct detection, through peak shifts, of the degree of crystallinity [7].

This chapter describes the use of the AFM to acquire images of polymer films with and without a commonly used plasticizer, triethyl citrate (TEC), and betamethasone valerate (BMV), a model drug most commonly used for inflammatory skin conditions. Films of all compositions appear homogeneous with no obvious occurrence of phase separation or drug crystallinity. This supports the use of TEC as an effective plasticizer as it distributes evenly within the polymer network forming the film. The lack of crystallization in all films confirms that the presence of the plasticizer is not affecting the state of the drug.

AFM nanoindentation, to determine the material nature of the samples and their elastic moduli, was carried out. The samples showed viscous-elastic-plastic behaviour and elastic moduli were extracted using both the Hertzian model and an adapted

H. Garvie-Cook, *Novel (Trans)dermal Drug Delivery Strategies*,
Springer Theses, DOI 10.1007/978-3-319-28901-4_4

Oyen & Cook model, as described in Sect. 3.1.3.4. The calculated elastic moduli were found to decrease with increasing plasticizer content.

Raman spectroscopy of the constituents of the polymeric films (polymers, the plasticizer and the drug substance) revealed characteristic spectral peaks by which they could be identified. These peaks were used to determine the distribution of these components from the measured Raman chemical maps of films containing plasticizer and the drug. This information was on a larger scale (with a lower resolution) than that obtained using AFM but was complementary, showing the homogeneity of the plasticizer and drug distribution within the films.

4.1 AFM Imaging

Images of polymeric FFS, cast on cleaned glass slides, were acquired in AFM tapping mode. Both Eudragit and Klucel films, incorporating 0, 20 and 40 % TEC, were prepared and the images of these films are shown in Fig. 4.1.

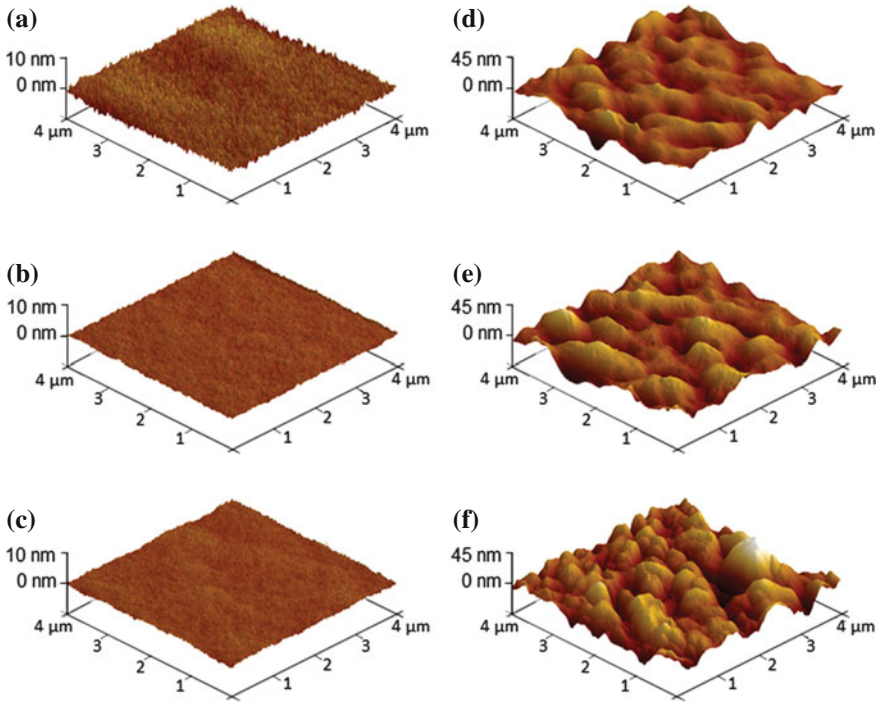

Fig. 4.1 3D AFM images of polymeric films with 0, 20 and 40 % TEC plasticizer, cast onto glass microscope slides, at scan sizes of $4 \times 4\ \mu m^2$: **a–c** Eudragit films with 0, 20 and 40 % TEC, respectively, and **d–f** Klucel films with 0, 20 and 40 % TEC, respectively

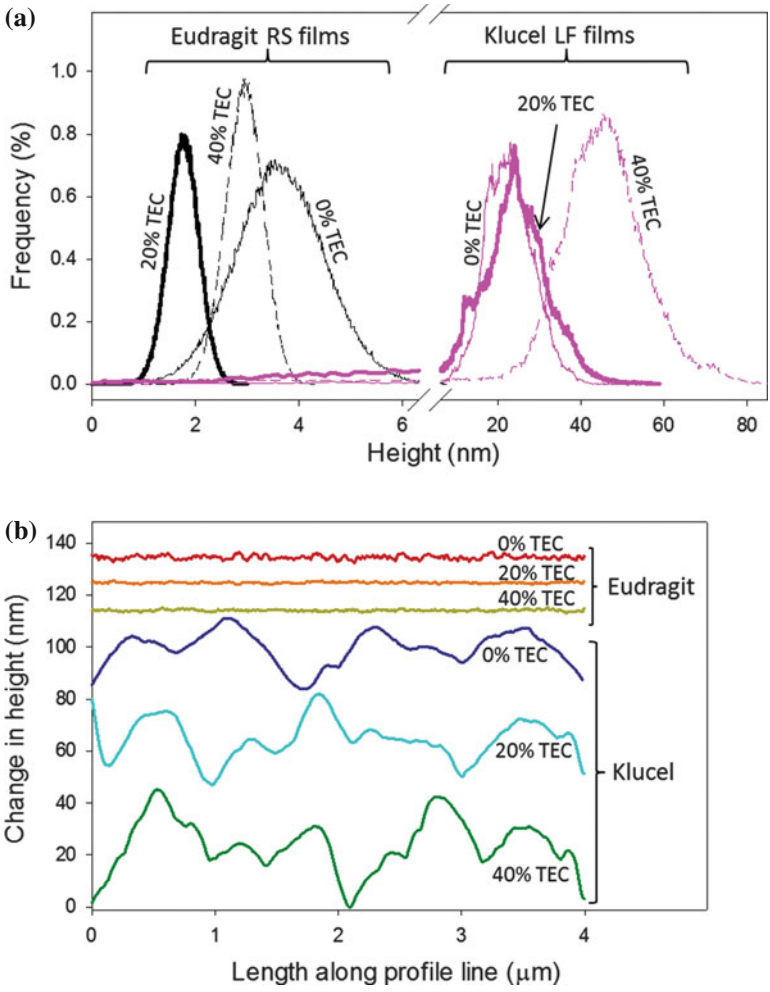

Fig. 4.2 **a** Histograms of AFM image feature height frequency, and **b** the change in height along one line of AFM images of films incorporating 0, 20 and 40 % TEC plasticizer. Height profiles in (**b**) are offset to facilitate comparison

Histograms of the heights of features in AFM images (Fig. 4.2a) represent the range of features observed. These histograms were produced by determining the number of features over certain threshold heights. Height profiles along one line of the image are also shown (Fig. 4.2b) to further support the information in the histograms.

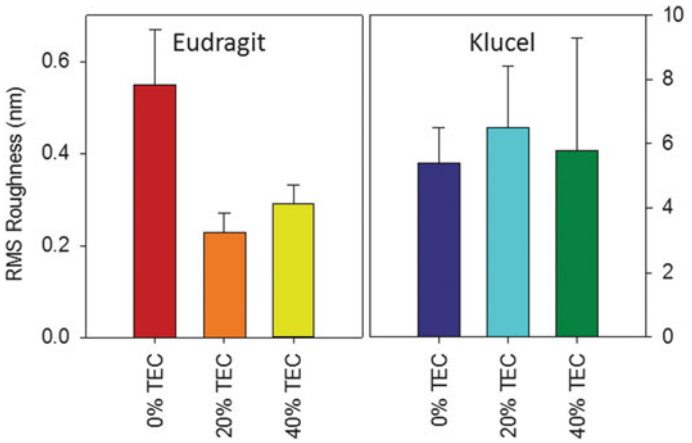

Fig. 4.3 RMS roughness (+ standard deviation) of Eudragit and Klucel films, with 0, 20 and 40 % TEC, determined from three AFM tapping mode images of each film

Root mean square (RMS) average roughness provides another description of the features observed in AFM images. It is the average of height deviations from a mean image data plane.

Eudragit films without TEC (Fig. 4.1a) show small structural features, with heights just below 4 nm (Fig. 4.2). The heights of these features decrease with increasing TEC content and the films were smoother when 20 and 40 % TEC (Fig. 4.1b, c) were incorporated. The RMS roughness (R_q) of three films of each composition, cast in the same way, decreased from 0.55 ± 0.12 nm, in films without TEC, to 0.23 ± 0.04 and 0.29 ± 0.04 nm in films with 20 and 40 % TEC, respectively. The changes in RMS roughness with increasing plasticizer content are shown in Fig. 4.3.

Klucel films without TEC show larger structural features than those observed in the equivalent Eudragit film, with heights of approximately 20 nm (Fig. 4.2). The root mean squared roughness of this film is 5.4 ± 1.1 nm. As the content of TEC increases, the heights of the structural features increase to approximately 45 nm in films incorporating 40 % TEC (Fig. 4.2a), but the RMS roughness did not change: 6.5 ± 1.9 and 5.8 ± 3.5 nm for films incorporating 20 and 40 % TEC, respectively (Fig. 4.3).

Polymeric films form from the FFS as the solvent evaporates from the solution. Ethanolic solutions of both Eudragit and Klucel are clear and are therefore believed to be polymeric solutions, rather than dispersions. In solution, polymer chains are highly mobile but come into close contact as the solvent evaporates, eventually forming a film as shown below. The rate of film formation and the structure of the formed film depend on the rate of solvent evaporation and the presence (or not) of a plasticizer.

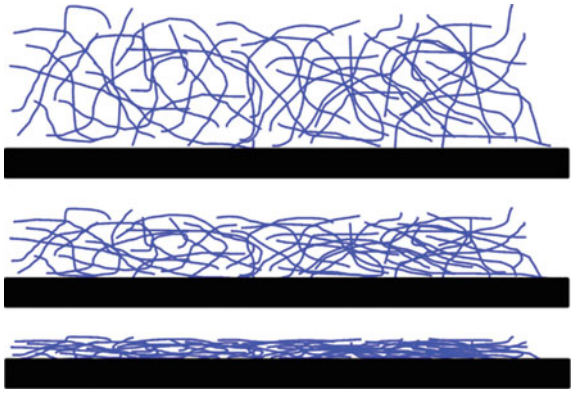

As the solvent evaporates, the mobile polymer chains move closer together until they form rigid polymer-polymer contacts. An effective plasticizer increases the flexibility of the film by decreasing the number of polymer-polymer contacts and therefore the rigidity of the formed structure [3, 9–11]. Ideally, the drug is either dissolved in the polymer or in an amorphous state within the polymeric network [12, 13].

There are no signs of phase separation or drug crystallization in the AFM images of any film, indicating that, when present, TEC and BMV were distributed evenly throughout the film. TEC has therefore effectively plasticized the formed films. The observed homogeneity of the films is an important quality as inhomogeneous polymer coatings can cause more rapid drug release from parts of the film [10]; equally, the formation of drug crystals decreases the eventual bioavailability of the drug [1].

The roughness of Eudragit films (with and without drug) decreases with increasing plasticizer content. The presence of plasticizer in the polymer network provides "gap-fillers", which result in a smoother film [5]. The same decrease in roughness with plasticizer content was not observed for Klucel films which did not contain the drug substance. This may be due to the larger molecular weight of the Klucel (95,000 g mol^{-1}), relative to the plasticizer (276 g mol^{-1}), and compared to Eudragit (32,000 g mol^{-1}), resulting in a lower change in roughness.

4.2 AFM Nanoindentation

4.2.1 Deformation Behaviour

Nanoindentation of films of different composition was carried out using AFM probe tips. The raw data from the indentation procedure (deflection in volts as a function of displacement of the AFM cantilever from its original vertical position) was converted to the deformation of the sample according to the applied load using the procedure

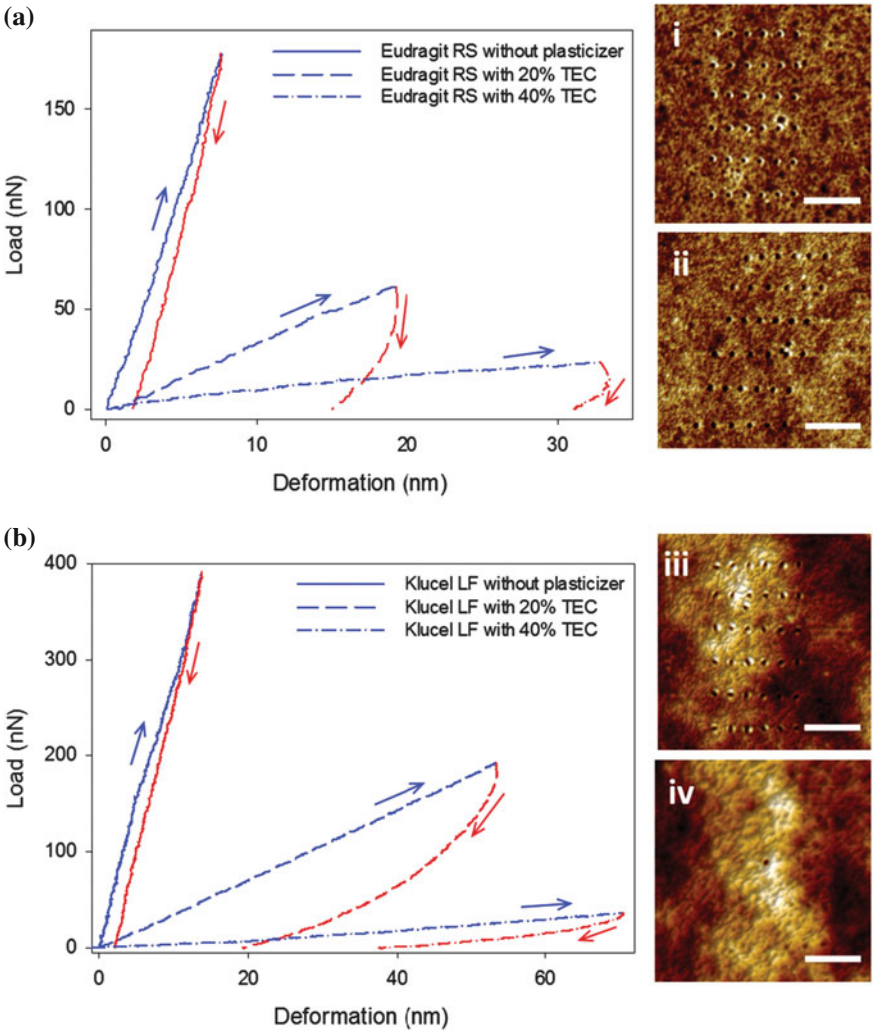

Fig. 4.4 Load as a function of deformation during indentation of films with and without plasticizer (TEC): **a** Eudragit with 0, 20 and 40 % TEC, and **b** Klucel with 0, 20 and 40 % TEC. *Blue* and *red lines* are data collected as the load was increased and decreased, respectively. 2D AFM images of (*i–ii*) Eudragit with 0 and 20 % TEC, and (*iii–iv*) Klucel with 0 and 20 % TEC were taken after indentation. Scale bar represents 0.5 μm. Indents are less obvious in (*iv*) due to the more viscous nature, and the greater roughness of the sample, as compared to (*ii*)

described in Sect. 3.1.3. Examples of the resulting data from samples incorporating 0, 20 and 40 % TEC (Fig. 4.4) clearly reveal the impact of plasticizer incorporation. The greatest load is required to deform (and the steepest loading curve is obtained for) Eudragit films without TEC (Fig. 4.4a). As TEC content increases, the load

required to deform the sample by a given amount decreases, showing the softer nature of films. Similar behaviour, with increasing TEC content, was observed for Klucel films (Fig. 4.4b).

The variation of deformation with load on the polymeric films reveals the indentation behaviour of the samples. This allows a model to be selected that accounts for the deformation behaviour of the samples and allows determination of their elastic moduli [14]. Large hysteresis, and a residual deformation when the load has been removed, were observed (Fig. 4.4), implying that some plastic deformation occurred during indentation. This residual deformation can be observed in AFM images of the films taken after indentation (Fig. 4.4i–iv).

4.2.1.1 Viscosity

Viscous behaviour can be assessed using the unloading data obtained during indentation. For Eudragit films with 20 and 40 % TEC, the hysteresis between the loading and unloading data remains large until the load is entirely lifted and a residual deformation is left (Fig. 4.4a). In Klucel films with 20 and 40 % TEC, this hysteresis is lower and the depth of the residual deformation left after the load is lifted is smaller (Fig. 4.4b). This difference shows the greater reversibility (i.e., the more elastic nature) of Klucel films containing TEC than the corresponding Eudragit films.

Viscous deformation was investigated by varying approach rate and surface delay. The approach rate is the speed at which the AFM probe is brought down towards and pushed into the sample. The probe is then retracted from the sample at the same speed. Approach rates of 4 and 16 nm s^{-1} were used for the indentation of all films investigated. Example indentation loops acquired at these different approach rates are shown in Fig. 4.5.

Less deformation, during loading and unloading, was observed for indents carried out at approach rate of 16 nm s^{-1} than those using 4 nm s^{-1}. Using Fig. 4.5 as an illustrative example, at a load of 30 nN, the deformation during loading of the Eudragit film without plasticizer was lower (1.6 nm compared to 2.2 nm) at the higher approach rate. This is also reflected in the behaviour of Klucel films with 40 % TEC; the deformations during loading were 76 and 121 nm for approach rates of 16 and 4 nm s^{-1}, respectively. When approaching at a higher rate, the sample provides a greater resistance to deformation as there is less time for viscous relaxation to occur [15]. The deformation at a given load is therefore lower.

There was less hysteresis between the approach and retract curves when a higher approach rate was used. In Fig. 4.5, the difference in deformation between the approach and retract curves at a load of 30 nN was 2 and 5 nm at approach rates of 16 and 4 nm s^{-1}, respectively for Eudragit films without plasticizer. For Klucel films with 40 % TEC, the hysteresis between the approach and retract curves at a load of 30 nN was 44 and 51 nm at approach rates of 16 and 4 nm s^{-1}, respectively. Again, this difference is due to the time allowed for more viscous relaxation to occur at a slower approach rate.

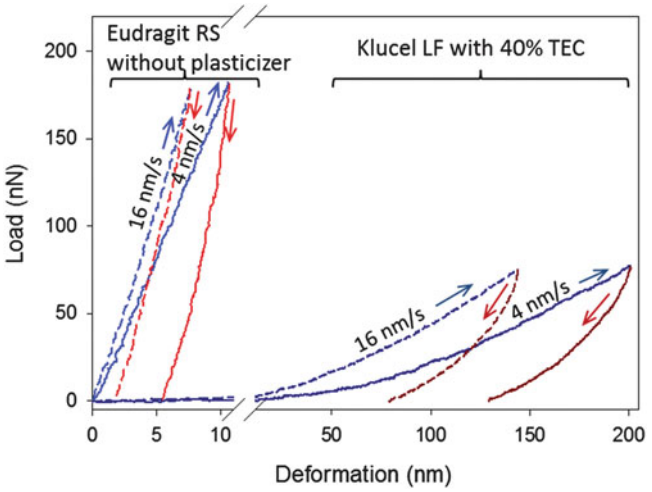

Fig. 4.5 Load as a function of deformation during indentation of a Eudragit film without plasticizer, and a Klucel film incorporating 40 % TEC, at approach rates of 4 nm s^{-1} (*solid lines*) and 16 nm s^{-1} (*dashed lines*)

Another indication of viscous deformation is the appearance of a "nose" in the initial unloading data of the samples. Even during unloading, the deformation of the sample may still increase (the "nose" in the data) if the sample shows viscous behaviour. In this case, the rate that the sample creeps under the applied load (due to its viscosity) is greater than the unloading rate. An example of this initial increase in deformation during unloading can be seen in Fig. 4.4a: the viscous nature of Eudragit films with 40 % TEC is sufficient that the probe continues to sink into the sample even after the load has begun to be lifted. The gradient of the initial unloading portion can therefore be used to assess the viscosity of the sample.

The gradient of the "nose" was calculated for the data shown in Fig. 4.4. The values for the initial unloading portions (the first 25 % of the data) for Eudragit films containing 0, 20 and 40 % TEC were 36, 66 and –15 nN/nm, respectively. As the plasticizer content of the films increases, the probe sinks into the sample at a greater rate during unloading. This causes the gradient to increase and then to become negative. Eudragit films with 40 % TEC therefore show a greater viscous nature than samples without plasticizer. The gradients of the initial unloading portions of Klucel films were also calculated. The values were 38, 15 and 2 nN/nm for films incorporating 0, 20 and 40 % TEC, respectively. In this case, the gradient becomes shallower, i.e., less unloading is required for a given decrease in deformation, as expected from the softer nature of samples containing TEC, and an obvious "nose" is not observed. Eudragit films therefore show more viscous deformation than Klucel films when TEC is incorporated. The molecular weight of Eudragit is lower than that of Klucel (32,000 compared to 95,000 g mol^{-1}) and the degree of its polymer chain entangle-

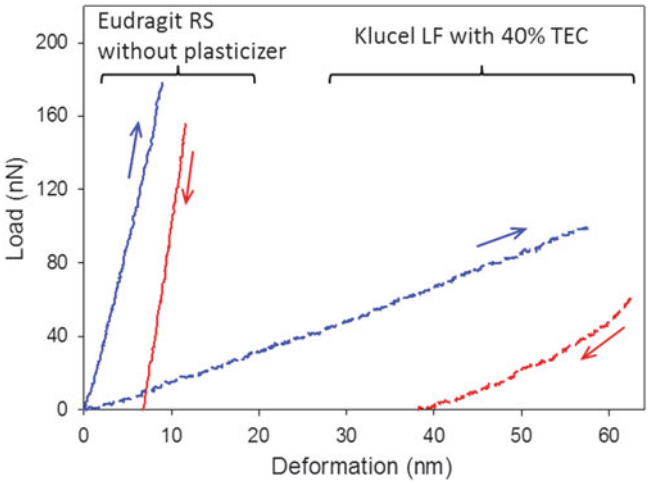

Fig. 4.6 Load as a function of deformation during indentation of a Eudragit film without plasticizer (*solid lines*), and a Klucel film incorporating 40 % TEC (*dashed lines*). A delay of 10 s at maximum load and an approach rate of 16 nm s^{-1} were used in these measurements

ment is less. This results in greater chain mobility and the more viscous deformation observed in Eudragit films is emphasized when TEC is incorporated [13].

Delays of 0 and 10 s were used to assess the creep of the probe during indentation. During this delay, the cantilever is held at its maximum vertical displacement, at which point the probe tip imposes the greatest load on the sample. In purely elastic-plastic samples, deformation would not change during this delay. When a surface delay of 10 s was used during the indentation of Eudragit films without plasticizer and Klucel films with 40 % TEC, both of which show viscous behaviour, an increase in the deformation of the sample at the maximum load is observed (Fig. 4.6). During the delay, the probe sinks further into the sample, even though the cantilever is being held at a fixed position. The deflection of the cantilever, and therefore the measured load, decreases during the delay as the deformation caused by the samples' viscosity increases. In the case of Eudragit films without plasticizer, the load decreases to 87 % of its original value before the hold period. The load decreases more, to 61 % of its original value, for Klucel films with 40 % TEC. This is consistent with the more viscous nature of the sample containing TEC plasticizer. An increase in the viscous behaviour of polymeric films with increasing plasticizer content has previously been observed in hydroxypropylmethylcellulose films plasticized with glycerol and polyethylene glycol [3]. This was attributed to the reduction in rigid polymer-polymer contacts when plasticizer is incorporated.

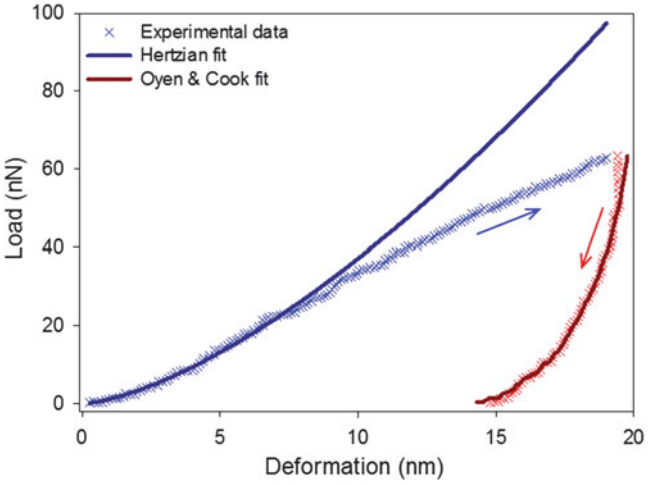

Fig. 4.7 Fits of the Hertzian and Oyen & Cook models (*upper* and *lower solid lines*, respectively) to the experimentally measured load as a function of deformation (*crosses*) during indentation of a Eudragit film incorporating 20 % TEC

4.2.2 Extraction of Elastic Modulus

4.2.2.1 Comparison of Hertzian and Oyen and Cook Models

The elastic moduli of polymeric films of different compositions were determined using the methods described in Sect. 3.1.3.4. Both Hertzian and Oyen & Cook models were fitted to experimental indentation data, and examples are shown in Fig. 4.7.

The Hertzian model describes the behaviour of purely elastic media. As shown in Sect. 4.2.1, the polymeric films under investigation are not purely elastic. However, for very small deformations, the Hertzian model is often considered to be a reasonable approximation for samples which are not purely elastic.

Loading data within the initial 5–20 % of experimental points was fitted to extract the elastic modulus using the Hertzian model. The deformation here was assumed to be essentially elastic. It is noted that the range chosen excludes the initial loading data when the indentation process is most prone to noise [16]. This also resulted in the most consistent results with sufficient data points for all samples to provide a reasonable fit. The Hertzian model explains well the first 5–20 % of data but then diverges predicting a lower deformation at a given load than is seen experimentally. This is expected as only the elastic deformation of the sample is modelled while, at greater loads, plastic deformation and viscous deformation become more apparent. The experimental deformation of the sample at a given load is therefore higher than that predicted by the purely elastic Hertzian model.

The Oyen & Cook model, which takes into account the viscous-elastic-plastic behaviour of the sample, was fitted to the central 75 % of experimental data. Elastic

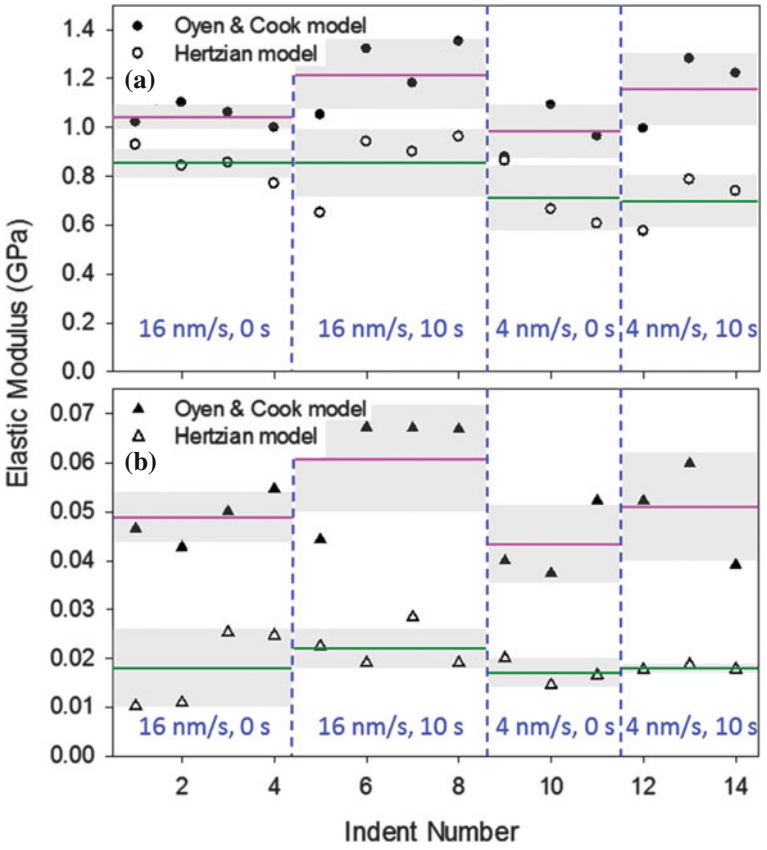

Fig. 4.8 Examples of Oyen & Cook and Hertzian model-calculated elastic moduli for (**a**) Eudragit without plasticiser, and (**b**) Klucel incorporating 40 % TEC, determined under four different indentation conditions: approach rate of 16 nm s^{-1} and 0 s delay, 16 nm s^{-1} and 10 s, 4 nm s^{-1} and 0 s, 4 nm s^{-1} and 10 s. Averages of Oyen & Cook and Hertzian moduli for each indentation condition are shown as *pink* and *green lines*, respectively. Areas shaded in grey represent the standard deviations of these averages

moduli values calculated using the Oyen & Cook model were consistently higher than those obtained from the Hertzian model (the comparison between the results for two different films is shown in Fig. 4.8). It follows that the data range fitted by the Hertzian model included some non-linear plastic and viscous deformation and the model therefore predicted a greater elastic deformation than was actually occurring (and hence resulted in a lower elastic modulus). This was verified by varying the data range over which the elastic modulus was determined (an example of this is shown in Table 4.1). The narrower the range of data points fitted (i.e., those closest to the start of the indent), the higher the derived elastic modulus. The deformation at these initial points is more likely to be purely elastic and the elastic modulus extracted is higher, and in agreement with the Oyen & Cook prediction. As the fitted data range

Table 4.1 Elastic modulus of a Eudragit film without plasticizer determined from fits of one indentation loop to the Hertzian model using different data ranges

Fitted range (% of loading data)	Hertzian elastic modulus (GPa)
1–16	1.04
3–18	0.972
5–18	0.941
5–20	0.927
5–30	0.887
5–40	0.823

increases and includes more points from the later stages of the indent, the Hertzian elastic modulus decreases. Here, the viscous and plastic contributions to deformation are greater and it is likely, therefore, that the Hertzian model underestimates the elastic modulus of the sample.

The effect of approach rate and the impact of a delay on the fitted Hertzian and Oyen & Cook elastic moduli were determined (Fig. 4.8) for each indentation condition (i.e., 16 nm s^{-1} and 0 s delay, 16 nm s^{-1} and 10 s delay, etc.). The elastic moduli calculated with the Oyen & Cook model were not significantly different over all the indentation conditions used. This model successfully accounts therefore for the viscous and elastic deformations, observed in Fig. 4.4, that occur during unloading. The values of elastic moduli determined from the Hertzian model also showed no obvious dependence on approach rate and surface delay suggesting that the contributions of viscous and plastic deformation are insignificant in the range of experimental conditions examined.

The variation of the Hertzian and Oyen & Cook model-calculated elastic moduli as a function of the maximum (peak) load used during indentation is shown in Fig. 4.9

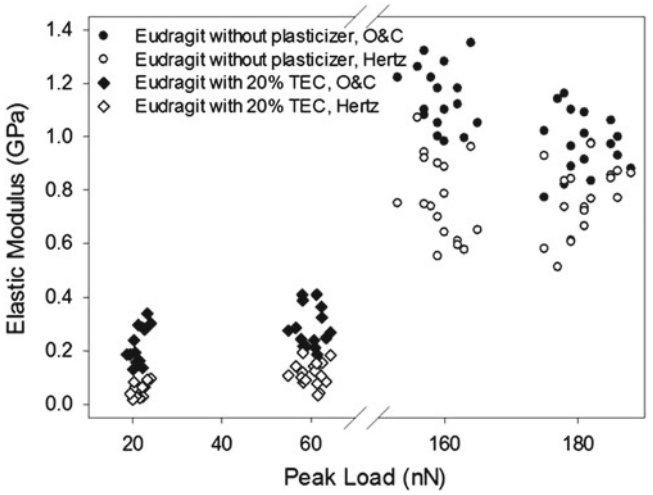

Fig. 4.9 Examples of Oyen & Cook and Hertzian elastic moduli for Eudragit without plasticizer and Eudragit with 20 % TEC as a function of the peak load imposed during indentation

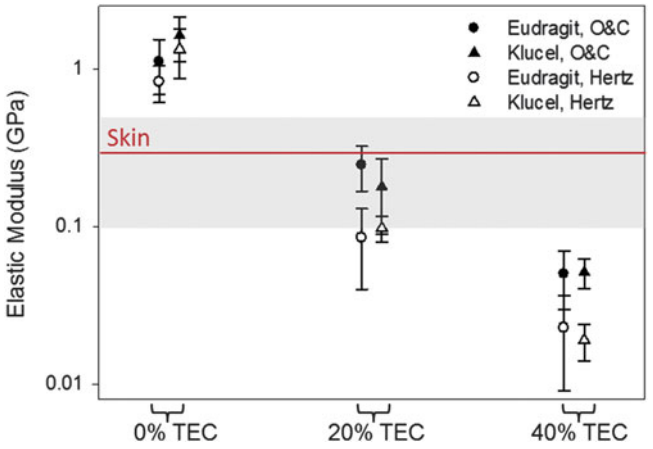

Fig. 4.10 Oyen & Cook and Hertzian model-calculated elastic moduli of Eudragit and Klucel films without and with 20 and 40 % plasticizer. The data shown are the means and standard deviations determined from three different samples of each film and a minimum of eight indents per sample. The elastic modulus of skin [17], determined under similar indentation conditions, is shown as a *horizontal line* for comparison, with the standard deviation shown in *grey*

for Eudragit films with and without 20 % TEC. The Hertzian elastic moduli did not vary with peak load for either film, behaviour characteristic of an ideal elastic material [7]. Elastic modulus calculated using the Oyen & Cook model appeared to decrease somewhat at higher loads, where the viscous deformation of the sample will become more prevalent. This suggests that the model may not have completely accounted for the viscous behaviour of the films.

Finally, all elastic moduli calculated for all films investigated were unchanged when the drug substance (1.2 % w/w) was incorporated (data not shown).

4.2.2.2 Variation with Plasticizer Content

Elastic moduli of Eudragit and Klucel films, calculated using Hertzian and Oyen & Cook models, as a function of TEC content, decreased with increasing plasticizer content, as expected (Fig. 4.10) [4]. Although the absolute, calculated values of the two models differed, the large decrease in modulus with the incorporation of plasticizer is patently clear.

Similar behaviour has been observed in other films incorporating plasticizer: a decrease in elastic modulus in hydroxypropylcellulose hot-melt extruded films when plasticized using polyethylene glycol [18], an increase in flexibility and elasticity when polyvinyl alcohol films incorporated glycerine as a plasticizer [19], and a reduction in the tensile strength of Eudragit® L 100-55 films plasticized with TEC [20]. The elastic modulus of human skin, approximately 0.3 GPa [17], is lower than the moduli of unplasticized Eudragit and Klucel films. A plasticizer content of 20 %

TEC must be introduced into the films to bring their elastic moduli down to that of skin and to ensure intimate and prolonged contact between the skin and the topically applied film. Plasticizer within the film decreases polymer-polymer contact, and the mobility of the polymer chains is therefore increased (and the films have a lower elastic modulus [4]). With increasing plasticizer, the effect is magnified.

The effects of plasticizer on drug release from polymer films have previously been reported for tablet coatings [10], and strongly depended on the plasticizer used (hydrophilic or lipophilic). Drug release from films of the same composition as those studied here increased with with increasing TEC content [21], presumably due to enhanced difusivity within the polymer network [13].

4.3 Raman Micro-Spectroscopy

4.3.1 Constituent Spectra

Raman spectra of the constituents of polymeric FFS were initially acquired (Fig. 4.11) to determine characteristic peaks by which they could be identified in spectroscopic maps of the formed films. Characteristic peaks for BMV and TEC were identified at 1659 and 1734 cm^{-1}, respectively. The peak for BMV was distinct from any polymer or plasticizer peak and could therefore be used to map the drug within films of both polymers. The 1742 cm^{-1} peak for TEC could be clearly distinguished in the Klucel

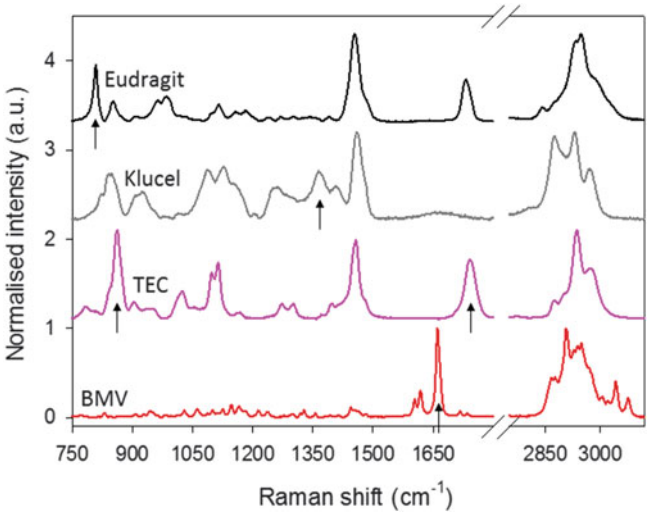

Fig. 4.11 Raman spectra of the constituents of polymeric films: Eudragit, Klucel, TEC and BMV. Spectra are normalised according to the maximum intensity within the two ranges shown. *Arrows* indicate the positions of characteristic peaks for each of the constituents

films but overlapped with a Raman signal from the polymer in Eudragit films. In these films, therefore, the peak intensity at 857 cm^{-1} was used to map the distribution of TEC. Peaks which were characteristic of the polymers Eudragit and Klucel were identified at 813 and 1358 cm^{-1}, respectively.

Raman chemical mapping was performed at a high spatial resolution to provide comparison with AFM images. The Raman signal obtained during mapping originated from an area of approximately $1 \times 1\ \mu m^2$. Maps were acquired of Eudragit and Klucel films, incorporating 20 % TEC and 1.2 % BMV, respectively. Spectra from the maps were processed by subtracting the background. The software used assumed the same background, as defined in one spectrum, for every pixel of the map.

The position of the characteristic peaks of TEC shifted when the plasticizer was incorporated into Eudragit and Klucel films, as opposed to in its powder form. Over the mapped area of Eudragit and Klucel films with 20 % TEC and 1.2 % BMV, the TEC peak positions were $858.3 \pm 0.1\ cm^{-1}$ and $1729.5 \pm 0.2\ cm^{-1}$, respectively. In both cases, therefore, the position of the peak decreased, suggesting that the environment in which the scattering TEC molecules were contained was altered. As no inhomogeneities were observed in either AFM images or Raman concentration maps (see Sect. 4.3.2), it is likely therefore that TEC was dispersed within the network provided by the film-forming polymers.

A similar effect was observed when the drug was incorporated into polymeric films; the characteristic peak of BMV shifted to 1669.0 and 1666.9 cm^{-1} in Eudragit and Klucel films (without TEC), respectively. This is further discussed in Sect. 4.3.3.

4.3.2 Mapping Concentration

The focus of the Raman microscope objective, and therefore its ability to collect the scattered radiation, is affected by changes in the height of the film across the mapped area. If the sample becomes out of focus, a lower intensity and background will be collected. Maps of the intensities of characteristic peaks of the polymer, plasticizer and drug within Eudragit films with 20 % TEC and 1.2 % BMV were similar, suggesting that changes in the topography of the film, rather than changes in the film's chemical distribution, explained the distribution observed.

To account for changes in sample height, spectra acquired along a line of each map were analysed. The intensities of characteristic peaks of polymer, plasticizer and drug were determined for each of these spectra then normalised according to each component's maximum intensity in the line of spectra analysed (Fig. 4.12a). The intensities of all characteristic peaks decreased to a minimum at a distance of approximately 9 μm along the line and then increased progressively to a maximum value observed at approximately 26 μm.

Prior to the analysis of peak intensities, background was subtracted from the individual spectra which formed the map. The Wire software, which was initially used to subtract background, assumed the same background spectrum over the mapped area. The variation in background intensities due to sample focus were therefore not

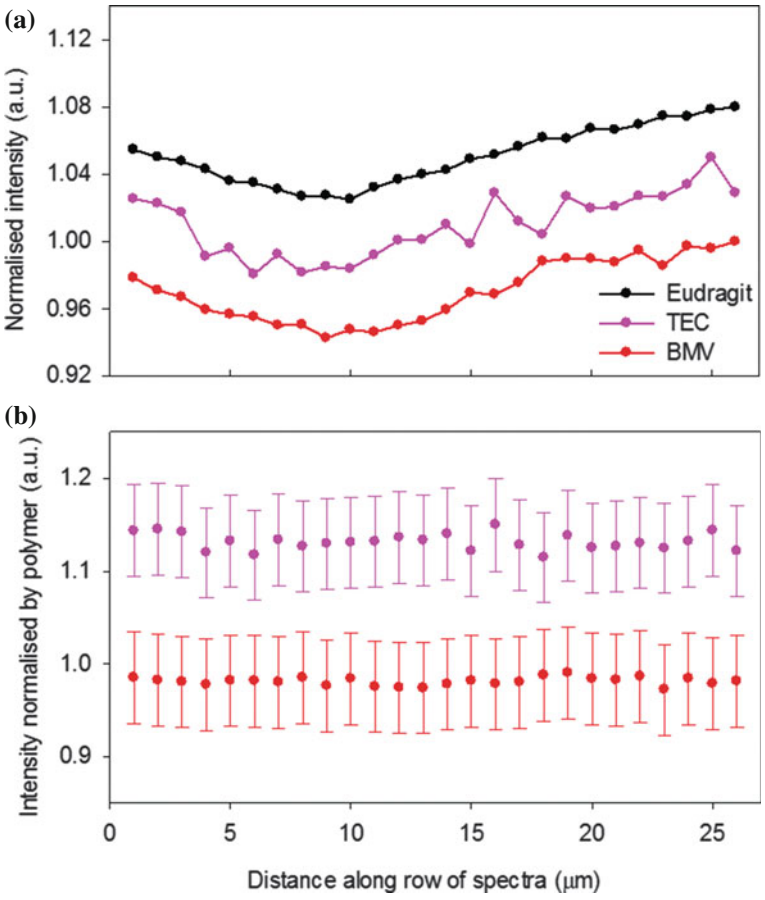

Fig. 4.12 **a** Raman peak intensities of Eudragit, TEC and BMV along a row of 26 spectra of a Eudragit film incorporating 20 % TEC and 1.2 % BMV. Intensities were normalised according to their maximum along this row. **b** Peak intensities of TEC and BMV were then divided by the intensities of the polymer peak. The maximum intensities of these divided signals were then defined as 1. Errors were calculated using the standard deviation of TEC and BMV peak intensities after repeating manual background subtraction five times on one spectrum. Intensities are offset to facilitate comparison

accounted for. After the deduction of background, spectra from areas of the film which were more in focus had higher intensities, thought to explain the variation in intensity observed in Fig. 4.12a.

The polymer was assumed to be distributed evenly throughout the film and the intensities of the spectra along the line investigated were therefore divided by the polymer signal, to account for the change in background (Fig. 4.12b). To estimate an error on the intensity of characteristic peaks, the background signal of a spectrum of each film was defined, without using the automatic function in the Wire software, and

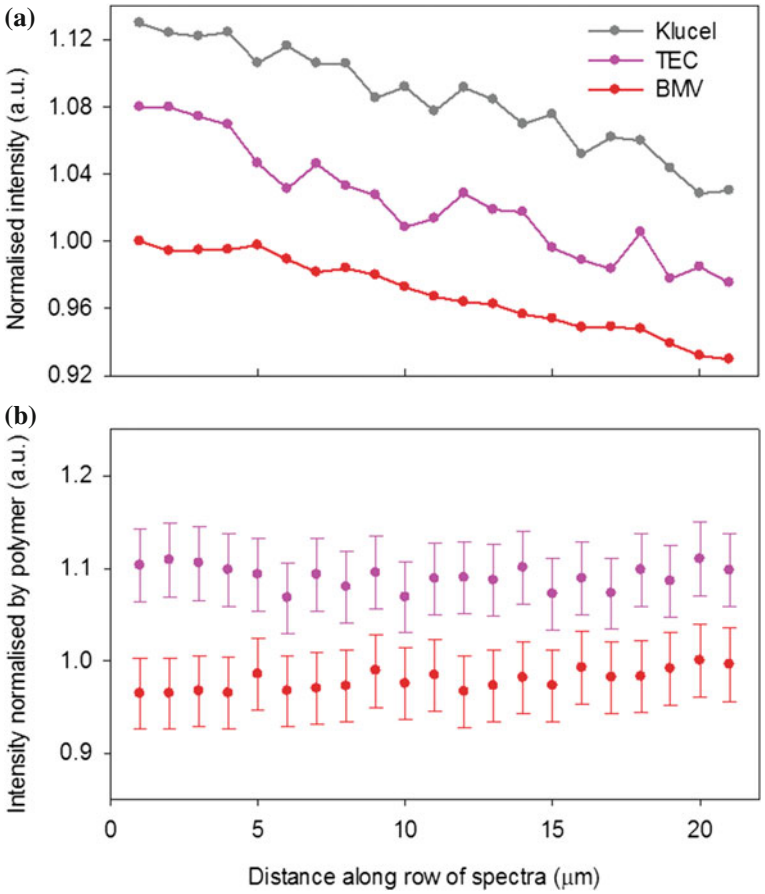

Fig. 4.13 **a** Raman peak intensities of Klucel, TEC and BMV along a row of 21 spectra of a Klucel film incorporating 20 % TEC and 1.2 % BMV. **b** Peak intensities of TEC and BMV were then divided by the intensities of the polymer peak. The maximum intensities of these divided signals were then defined as 1. Errors were calculated using the standard deviation of TEC and BMV peak intensities after repeating background subtraction five times on one spectrum. Intensities are offset to facilitate comparison

subtracted. Intensities of characteristic peaks were then deteremined and this process was repeated five times. The standard deviations of the determined intensities were used to calculate percentage errors. The concentrations of plasticizer and drug over the row of spectra from Eudragit with 20 % TEC and 1.2 % BMV were effectively constant (Fig. 4.12b) and TEC and BMV were therefore distributed evenly.

The same analysis was applied to maps of Klucel with 20 % TEC and 1.2 % BMV. In this case, the intensity of all characteristic peaks decreased in the same manner with increasing distance along the line of spectra, suggesting that the sample was became progressively out of focus (Fig. 4.13a). The polymer was again assumed to be

evenly distributed and the intensities of plasticizer and drug peaks were normalised according to its signal. The error was calculated in the same way as described above. The intensities of plasticizer and drug along the row of spectra analysed were, again, effectively constant (Fig. 4.13b). In both Eudragit and Klucel films incorporating TEC and BMV, plasticizer and drug were therefore distributed evenly, supporting the homogeneity observed in AFM images (Fig. 4.1).

4.3.3 Mapping the Physical State of the Drug

BMV was assessed spectroscopically in three physical forms and its characteristic peak (at spectral shifts of approximately 1650–1670 cm^{-1}) was determined. The three forms were crystalline (as provided by the supplier), as an amorphous film, formed by depositing a drop of an ethanolic solution onto a clean glass slide [22], and in solution (0.4 % w/w in ethanol), and the spectra acquired are in Fig. 4.14. The peak shifted from 1659 and 1663 cm^{-1} for crystalline and amorphous solid forms, respectively, to 1666 cm^{-1} for the dissolved compound.

The physical state of BMV across the films was then determined by mapping the frequency of its characteristic peak. In Eudragit films, the peak was observed at

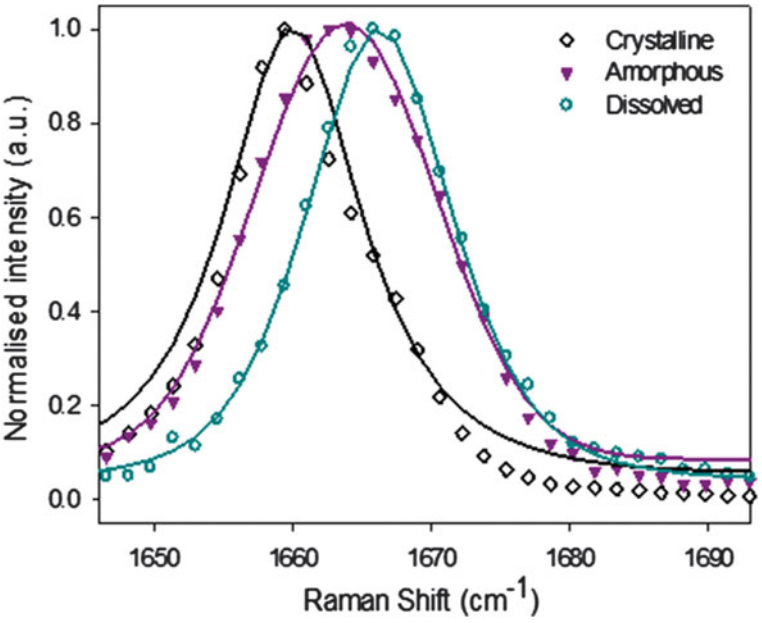

Fig. 4.14 Raman spectra of crystalline, amorphous and dissolved BMV. Spectra have been normalised to a maximum value of 1 within the range shown. Gaussian functions (*solid lines*) were fitted to spectral data points and used to determine the peak position

1667.8–1667.9 cm^{-1}; that is, a range much smaller than the difference, for example, between amorphous and dissolved drug, suggesting that BMV was dissolved and equally soluble throughout the mapped area of the film. The corresponding range of the peak position in a Klucel film incorporating 20 % TEC and 1.2 % BMV was 1665.9–1666.0 cm^{-1}, implying that BMV was dissolved but consistently less soluble across the mapped area. The positions of the BMV peaks were lower than those observed in Eudragit and Klucel films without TEC, suggesting that the incorporation of TEC has slightly reduced the solubility of the drug within the polymer film.

4.4 Film Formation on Skin

Section 4.2 describes the deformation behaviour and elastic moduli of topical films which were cast on glass slides and dried for 24 h at 30 °C. To determine whether the observed properties would vary when in situ on the surface of skin, AFM measurements of Eudragit films incorporating 0, 20 and 40 % TEC, prepared in three different ways, were carried out. The effects of the conditions of deposition and the substrate, i.e., glass or skin, were determined.

To examine the impact of changing the preparation method, films were cast onto either glass slides or excised porcine skin and dried for 6 hours at either room temperature or 30 °C. Example AFM indentation loops for these samples are in Fig. 4.15. The probe used for indentation had a smaller radius than those used before: 7 nm as compared to 21–80 nm. When a smaller probe is used, more plastic deformation occurs at a smaller load, making direct comparison of Fig. 4.15 with Fig. 4.4 less than straightforward. In general, however, the shapes of all of the load-deformation plots in these experiments were similar. For example, indentation of a Eudragit film incorporating 20 % TEC revealed similar viscous and plastic characteristics regardless of the preparation method used. Deposition and substrate parameters do not, therefore, appear to change the deformation behaviour of the films.

Variation in the films' mechanical properties, when prepared differently, can be quantified via their elastic moduli. As a sharper probe was used, more viscous and plastic deformation was observed, resulting in large hysteresis and residual deformation in all indentations. Elastic moduli were calculated by fitting the Hertzian model to small deformations; i.e., to the first 5–20 % of data acquired during loading (Fig. 4.16). Increasing the plasticizer content of the films resulted in a decrease in elastic modulus, as previously observed (Fig. 4.10). The preparation method had the most significant effect on the elastic moduli of Eudragit films with 40 % TEC, with those prepared at room temperature (on both glass and skin) having lower values than those prepared at 30 °C.

Elastic moduli of Eudragit films without plasticizer, and with 20 % TEC, prepared on glass slides at both 30 °C and room temperature, were higher than those which had been dried for 24 h at 30 °C. This difference is likely due to the smaller probe radius used for indentation. Nonetheless, the elastic moduli of the films were still observed to significantly decrease with increasing TEC.

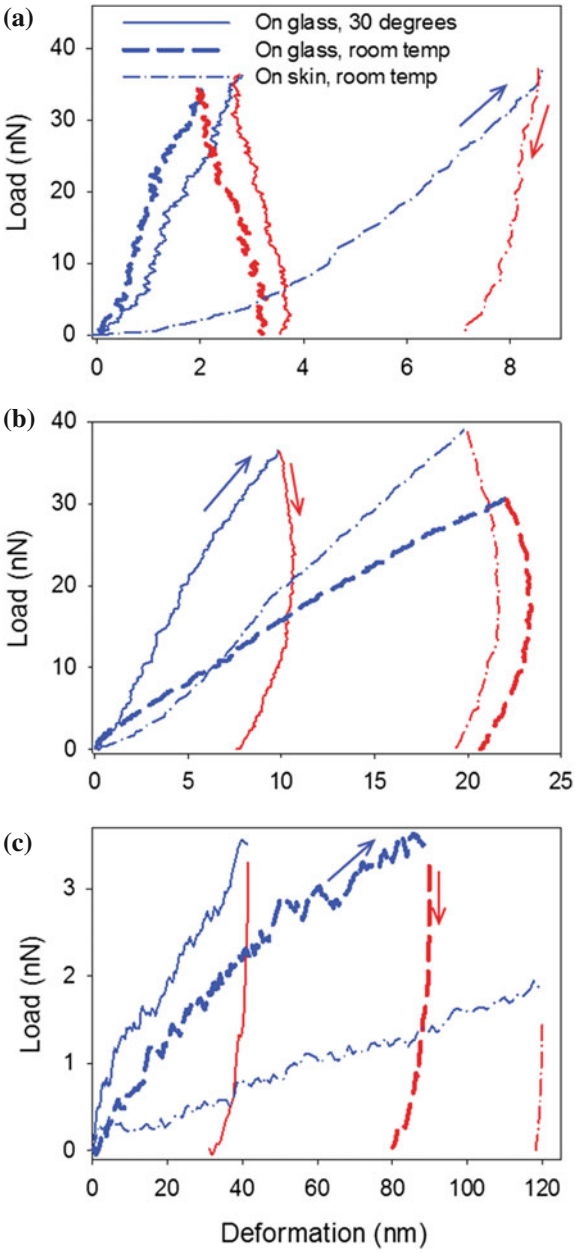

Fig. 4.15 Examples of load as a function of deformation during indentation of Eudragit films **a** without plasticizer, **b** with 20 % TEC, and **c** with 40 % TEC. Films were dried for 6 h on glass at 30 °C (*solid lines*), on glass at room temperature (*thick dashed lines*), and on skin at room temperature (*dash-dot-dashed lines*). *Blue* and *red lines* represent the data collected as the load was increased and decreased, respectively, as indicated by the arrows (color online)

Under the same load, the deformation of Eudragit films without plasticizer on skin was greater than that on glass, suggesting a softer sample (Fig. 4.15a). The elastic modulus of this sample, using the Hertzian model, was therefore lower (0.40 ± 0.14

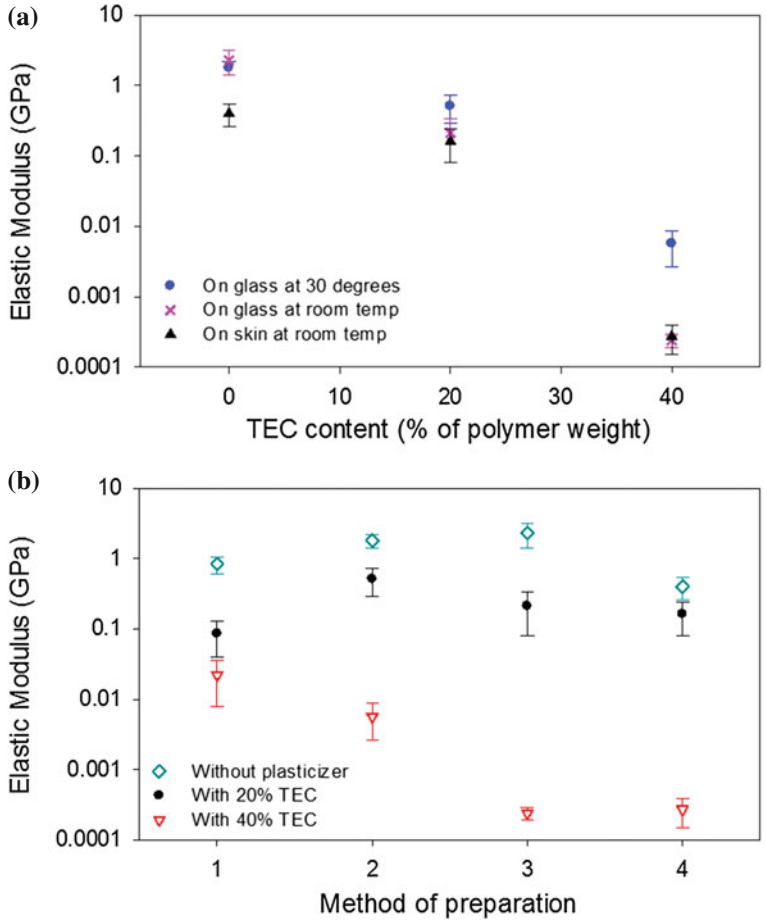

Fig. 4.16 Hertzian elastic moduli of Eudragit films (n = 8, ± standard deviation), without plasticizer and with 20 and 40 % TEC, prepared by different methods: **a** dried for 6 h on glass, at 30 °C and at room temperature, and on skin, at room temperature; **b** *method 1* dried for 24 h on glass at 30 °C, *method 2* dried for 6 h on glass at 30 °C, *method 3* dried for 6 h on glass at room temperature, and *method 4* dried for 6 h on porcine skin at room temperature

GPa) than seen before (Fig. 4.16b), implying that the film had been softened in some way by its interaction with the skin.

The elastic moduli of Eudragit films with either 20 or 40 % TEC, prepared on glass and on skin at room temperature, were not significantly different. It follows that the effect of TEC on the elastic modulus of the film is greater than the effect of skin on that which has no plasticizer incorporated.

The temperature of film formation affects the rate at which solvent evaporates from the FFS. Ethanol evaporation from these films occurs more quickly, of course, at higher temperatures. It has previously been observed that Klucel LF films require

longer times to form from ethanolic solutions when formed at 25 °C than at 30 °C (1.5 times longer) [23]. For the same drying time, a greater amount of ethanol will therefore be left in a film when formed at room temperature than at 30 °C. Solvent, like plasticizer, can reduce polymer-polymer contacts as the film forms, and more solvent molecules will therefore have a greater plasticizing effect and lower the elastic modulus, exactly as is seen for films containing 40 % TEC prepared at room temperature (relative to those formed at 30 °C) [3].

All indentations were performed on the surface of the film exposed to air. The properties of the bulk film and those at its interface with the skin may be different. While the former may be deduced from examination of the fracture surface [1, 5], assessment of film properties at its interface with the skin offers practical challenges that are difficult to overcome with AFM because the skin surface topography (its furrows and wrinkles) has a dimension much greater than the height range ($\leq$5.5 μm) of the instrument.

4.5 Summary and Conclusions

AFM imaging has been used to determine the change in topography of polymeric films, cast on glass slides and dried for 24 h at 30 °C, with increasing plasticizer (TEC) content. RMS roughness decreased with increasing plasticizer content for Eudragit films. A similar change in roughness was not observed for Klucel films with the same plasticiser content. The difference may be explained by the higher molecular weight of Klucel relative to that of Eudragit. AFM images revealed homogeneous films with no obvious phase separation or crystallization.

AFM indentation experiments characterised the viscous, elastic, plastic behaviour of the polymeric films. Viscosity was evaluated by varying the rate at which the probe indented the films and by the use of a delay at maximum load.

Elastic moduli of polymeric films were extracted from indentation loops using the Hertzian model, at small deformations, and an adapted Oyen & Cook model. Hertzian model-calculated elastic moduli were consistently lower than those based on the Oyen & Cook model. The range of elastic moduli determined under different indentation conditions, using both models, was less than the effect of plasticizer incorporation. Elastic moduli of polymeric films decreased with increasing TEC content, with the incorporation of 20 % plasticizer reducing this parameter to that of skin (and allowing, thereby, the likely potential for such films to flex when in situ on the surface of the skin without breaking).

Chemical mapping by Raman micro-spectroscopy of films incorporating TEC and BMV showed relatively uniform distributions of plasticizer and drug over the examined area, implying that no phase separation or crystallization occurred. Mapping the peak frequency of the signal from BMV, revealed that the drug was dissolved in the polymeric films and that it was more soluble in Eudragit than in Klucel.

The impact of film preparation method (glass versus skin substrate, room temperature versus 30 °C, and 6 versus 24 h drying time) was explored using Eudragit

films. In the absence of plasticizer, films formed on skin had lower elastic moduli than those prepared on glass, suggesting a possible plasticizing effect from moisture in the tissue. However, this was not observed when 20 or 40 % TEC was incorporated because the effect of the plasticizer overwhelmed that provoked by skin moisture.

References

1. M.E. Lauer, O. Grassmann, M. Siam, J. Tardio, L. Jacob, S. Page, J.H. Kindt, A. Engel, J. Alsenz, Atomic force microscopy-based screening of drug-excipient miscibility and stability of solid dispersions. Pharm. Res. **28**(3), 572–584 (2011)
2. Y.T.A. Tumer, C.J. Roberts, M.C. Davies, Scanning probe microscopy in the field of drug delivery. Adv. Drug Delivery Rev. **59**(14), 1453–1473 (2007)
3. M.E. Aulton, M.H. Abdulrazzak, J.E. Hogan, The mechanical-properties of hydroxypropylmethylcellulose films derived from aqueous systems. 1. The influence of plasticizers. Drug Dev. Ind. Pharm. **7**(6), 649–668 (1981)
4. J.W. McGinity, L.A. Felton, *Aqueous polymeric coatings for pharmaceutical dosage forms*, 3rd edn., Drugs and the pharmaceutical sciences (Informa Healthcare, New York, 2008)
5. M.E. Lauer, M. Siam, J. Tardio, S. Page, J.H. Kindt, O. Grassmann, Rapid assessment of homogeneity and stability of amorphous solid dispersions by atomic force microscopy-from bench to batch. Pharm. Res. **30**(8), 2010–2022 (2013)
6. A. Danesh, X. Chen, M.C. Davies, C.J. Roberts, G.H.W. Sanders, S.J.B. Tendler, P.M. Williams, M.J. Wilkins, Polymorphic discrimination using atomic force microscopy: Distinguishing between two polymorphs of the drug cimetidine. Langmuir **16**(2), 866–870 (2000)
7. S. Ward, M. Perkins, J.X. Zhang, C.J. Roberts, C.E. Madden, S.Y. Luk, N. Patel, S.J. Ebbens, Identifying and mapping surface amorphous domains. Pharm. Res. **22**(7), 1195–1202 (2005)
8. R. Price, P.M. Young, Visualization of the crystallization of lactose from the amorphous state. J. Pharm. Sci. **93**(1), 155–164 (2004)
9. A.Q.J. Low, J. Parmentier, Y.M. Khong, C.C.E. Chai, T.Y. Tun, J.E. Berania, X.M. Liu, R. Gokhale, S.Y. Chan, Effect of type and ratio of solubilising polymer on characteristics of hot-melt extruded orodispersible films. Int. J. Pharm. **455**(1–2), 138–147 (2013)
10. F. Lecomte, J. Siepmann, M. Walther, R.J. MacRae, R. Bodmeier, Polymer blends used for the aqueous coating of solid dosage forms: importance of the type of plasticizer. J. Controlled Release **99**(1), 1–13 (2004)
11. S.Y. Lin, C.J. Lee, Y.Y. Lin, Drug-polymer interaction affecting the mechanical-properties, adhesion strength and release kinetics of piroxicam-loaded eudragit-e films plasticized with different plasticizers. J. Controlled Release **33**(3), 375–381 (1995)
12. C.B. Wu, J.W. McGinity, Non-traditional plasticization of polymeric films. Int. J. Pharm. **177**(1), 15–27 (1999)
13. J. Siepmann, R.A. Siegel, M.J. Rathbone, *Fundamentals and applications of controlled release drug delivery*, Advances in delivery science and technology (Controlled Release Society, Springer, New York, 2012)
14. M.L. Oyen, R.R. Cook, A practical guide for analysis of nanoindentation data. J. Mech. Behav. Biomed. Mater. **2**(4), 396–407 (2009)
15. M.L. Oyen, R.F. Cook, Load-displacement behavior during sharp indentation of viscous-elastic-plastic materials. J. Mater. Res. **18**(1), 139–150 (2003)
16. D.C. Lin, D.I. Shreiber, E.K. Dimitriadis, F. Horkay, Spherical indentation of soft matter beyond the hertzian regime: numerical and experimental validation of hyperelastic models. Biomech. Model. Mechanobiol. **8**(5), 345–358 (2009)
17. J.D. Beard, R.H. Guy, S.N. Gordeev, Mechanical tomography of human corneocytes with a nanoneedle. J. Invest. Dermatol. **133**, 1565–1571 (2013)

18. M.A. Repka, J.W. McGinity, Physical-mechanical, moisture absorption and bioadhesive properties of hydroxypropylcellulose hot-melt extruded films. Biomaterials **21**(14), 1509–1517 (2000)
19. C. Padula, G. Colombo, S. Nicoli, P.L. Catellani, G. Massimo, P. Santi, Bioadhesive film for the transdermal delivery of lidocaine: in vitro and in vivo behavior. J. Controlled Release **88**(2), 277–285 (2003)
20. J.C. Gutierrez-Rocca, J.W. Mcginity, Influence of water-soluble and insoluble plasticizers on the physical and mechanical-properties of acrylic resin copolymers. Int. J. Pharm. **103**(3), 293–301 (1994)
21. K. Frederiksen, R.H. Guy, K. Petersson, Formulation considerations in the design of topical, polymeric film-forming systems for sustained drug delivery to the skin. Eur. J. Pharm. Biopharm. **91**, 9–15 (2015)
22. L.A. Wegiel, L.J. Mauer, K.J. Edgar, L.S. Taylor, Crystallization of amorphous solid dispersions of resveratrol during preparation and storage-impact of different polymers. J. Pharm. Sci. **102**(1), 171–184 (2013)
23. J. Bajdik, G. Regdon, T. Marek, I. Eros, K. Suvegh, K. Pintye-Hodi, The effect of the solvent on the film-forming parameters of hydroxypropyl-cellulose. Int. J. Pharm. **301**(1–2), 192–198 (2005)